Quality Improvement on Mechanical Properties of FDM 3D Printed Triply Periodic Minimal Surfaces (TPMS) Structure for Tissue Engineering Scaffold

Nor Hasrul Akhmal Ngadiman[1,2], Nur Syahirah Mustafa[1], Ahmed Ali Omar Alkaff[1], Muhammad Zameri Mat Saman[1]*

[1]Faculty of Mechanical Engineering, Universiti Teknologi Malaysia, 81310 Johor Bahru, Johor, MALAYSIA
[2]Department of Engineering, Faculty of Advanced Technology and Multidiscipline, Universitas Airlangga, Surabaya, 60115, INDONESIA
[*]norhasrul@utm.my

ABSTRACT

Bone tissue engineering is the best alternative to treat large-scale bone defects by developing a scaffold. Many attempts have been made, but mechanical properties are still a significant concern in producing a feasible scaffold. This study aims to optimize the parameters of Fused Deposition Modeling (FDM) 3D printing, specifically layer thickness, flow rate, filling density, and filling pattern. The objective was to improve the compressive strength and Young's modulus of the scaffolds, which are crucial for the effective regeneration of bone tissue. Through this study, it has been found that the significant parameters to develop a feasible scaffold are layer thickness, flow rate, and filling density. By optimizing the parameters to a layer thickness of 0.05 mm, a flow rate of 50%, and a filling density of 100%, the resulting scaffolds exhibited a compressive strength of 0.8329 MPa and a Young's modulus of 16.42 MPa. These values exhibit extraordinary mechanical durability. The study's importance lies in its contribution to advancing more efficient bone scaffolds. These tailored scaffolds, which balance mechanical strength and biological functions, can potentially enhance bone repair and regeneration. This study establishes a foundation to produce more dependable and effective scaffolds, ultimately improving bone regeneration treatments.

ISSN 1823-5514, eISSN 2550-164X

https://doi.org/10.24191/jmeche.v13i1.3755

Received for review: 2024-02-07
Accepted for publication: 2024-06-04
Published: 2024-11-15

Keywords: *Fused Deposition Modelling; Quality Improvement Optimization; Triply Periodic Minimal Surfaces; Bone Tissue Scaffold; Compressive Strength; Young's Modulus*

Introduction

The swift progress of 3D printing technology during the last ten years, namely in the field of biomedical applications, offers a revolutionary opportunity in the healthcare sector. This research seeks to investigate cutting-edge technology, with a specific emphasis on its use in the important field of bone tissue engineering scaffolds. The groundbreaking research conducted by several researchers has established the foundation, highlighting the immense potential of 3D printing in the production of complex organ models for surgical planning, customized implants, and particularly noteworthy, scaffolds that closely resemble organic tissues [1]-[3]. The focus of this study is to improve the comprehension and advancement of these support structures, particularly in the context of addressing the scarcity of organ donors.

The scaffolds used in bone tissue engineering, as described by Gregor et al. [1], are specifically designed to meet the unique requirements of each patient. These scaffolds serve a crucial role in facilitating the development of various types of tissues, such as bone and skin. Customization is vital for promoting both the development of new tissue and the necessary removal of metabolic wastes. Yan et al. [4] highlighted the need to have permeable yet structurally robust scaffolds since achieving this delicate equilibrium is crucial for their efficacy. The slow breakdown of the scaffolds, which is synchronized with the rate of tissue formation, highlights their intricate design and usefulness.

An emerging and captivating advancement in this domain is the concentration on Triply Periodic Minimal Surfaces (TPMS). TPMS structures have attracted considerable interest because of their distinctive characteristics of porosity and strength, which make them very appropriate for bone scaffolds [5]-[6]. These intricate geometric patterns create an ideal setting for bone regeneration by providing essential support, allowing for the proliferation of blood vessels and cells.

Yet, the difficulty is to effectively utilize 3D printing technology to create these intricate scaffolds based on TPMS. The mechanical qualities and printing settings have significant impacts on the quality and effectiveness of these scaffolds, as demonstrated by several previous studies [7]-[8]. To achieve uniformity in quality and fulfill the precise criteria for bone regeneration, it is essential to examine the printing process parameters and scaffold design thoroughly.

Hence, this study intends to thoroughly examine the parameters that affect the mechanical properties of bone scaffolds made from TPMS via Fused

Deposition Modeling (FDM) 3D printing. The discussion will include the complex relationship between the scaffold design, with a specific emphasis on TPMS structures, and the configurations of the 3D printing equipment. This study aims to create a structure for manufacturing superior bone scaffolds that utilize the distinctive benefits of TPMS to progress the field of bone tissue engineering. This finding represents not just a small advancement in tackling the lack of organ donors but also a significant leap in transforming the future of tissue engineering and regenerative medicine.

Methods

Development of the structure of the scaffold

The creation of a bone tissue scaffold structure is a multi-stage process, as depicted in Figure 1. The first step involves identifying distinct geometries and developing bone tissue scaffolds through CAD models. This design was executed using SolidWorks software, resulting in an initial model with dimensions of 76 x 76 x 76 mm. The model was then converted into a mesh file in.*stl* format, which is compatible with the slicing software used for configuring printing parameters, Ultimaker Cura. In the final stage, these designs were fabricated using an FDM 3D printer. Utilizing Ultimaker Cura, the dimensions of the scaffold were scaled down to 30 x 30 x 30 mm for printing. This procedure was undertaken to align with the suggestions put forth by several previous studies [9]-[11].

Material selection

This study focuses on the impact of mechanical properties on printing parameters, with a standardized selection of materials. Kuznetsov et al. [12] recommend the use of Polylactictide (PLA) material for scaffold fabrication due to its high biodegradability, absence of unpleasant odor when heated, and environmental friendliness throughout its lifecycle. PLA is suggested to enhance mechanical qualities by reducing internal stress. Additionally, Germain et al. [13] reported that the Food and Drug Administration (FDA) has approved PLA for biological applications. Alizadeh-Osgouei et al. [9] also highlight PLA's cost-effectiveness, user-friendliness, and wide availability. These attributes make PLA an ideal material for this investigation.

The shape and design of the scaffold

The TPMS scaffold design has been selected for this project, as illustrated in Figure 1. The design's capacity to withstand increased loads and stress determines the selection. Furthermore, some researchers have documented that a primitive construction has superior mechanical characteristics, reduced resource consumption, and necessitates mechanical anisotropy. According to De Aquino et al. [10] the primitive structure necessitated less support material

and had a quicker fabrication time. According to the authors, the maximum stress is attained before failure in both load test orientations. In addition, the construction has demonstrated the ability to withstand higher stress. The recorded amount has been determined to be threefold greater than the capacity that Gyroid and diamond scaffolds can handle.

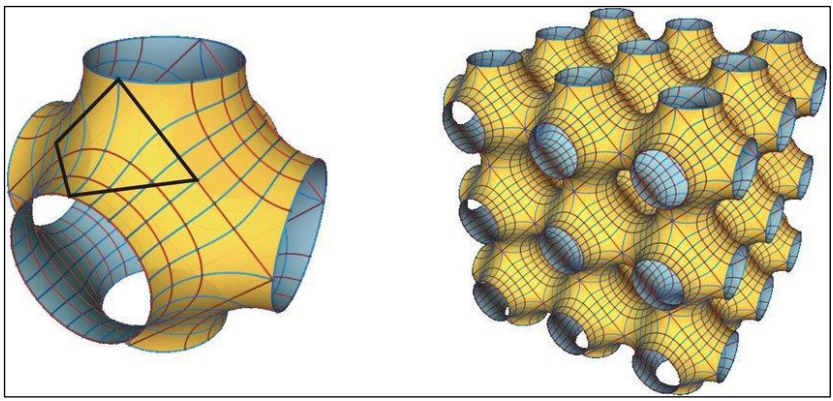

Figure 1: Primitive structure in CAD

Response Surface Methodology (RSM)

The Response Surface Methodology (RSM) was employed to identify the key elements and optimize parameter settings for the FDM 3D printing process, with the goal of achieving superior mechanical qualities in the scaffold. The response variable, which quantifies the mechanical property, is assessed based on compressive strength and Young's modulus. In general, the procedures for Response Surface Methodology (RSM) can be categorized into three primary components: factorial design for initial assessment, the steepest ascent/descent method for efficient movement towards the optimal region, and Central Composite Design (CCD) for establishing the relationship between variables and responses [14]-[16].

Table 1 displays the low and high levels for the four variables, as well as the range of each parameter. The selection of the range for each parameter (layer thickness, percentage of flow rate, filling density and filling pattern) was determined by an analysis of significant factors on the qualities of FDM 3D printer products, as identified in the literature review [6]-[7], [9], [11]-[12], [17]-[21].

Table 1: Factors and levels for the factors investigated

No.	Factor	Level		
		Low (-1)	**Center (0)**	**High (+1)**
1	Layer thickness (mm)	0.05	0.225	0.4
2	Flow rate (%)	50	60	70
3	Filling density (%)	40	70	100
4	Filling pattern	Line		Rectangular

Results

Design of Experiment (DOE) and Analysis of Variance (ANOVA)

Multiple variables were taken into account during the optimization analysis and Design of Experiments (DOE). This study incorporated two distinct categories of factors. The factors that are measured numerically are the thickness of the layer (*A*), the percentage of flow rate (*B*), and the percentage of filling density (*C*). The filling pattern (*D*) is the categorical component. The experimental layout of the designed studies has a total of 20 trials, which includes 2 center points. Two responses have been chosen, namely the compressive strength (response 1) and Young's modulus (response 2). Table 2 displays the experimental design. The samples were programmed using Cura software for slicing and generating the G-code, as depicted in Figure 2, and were fabricated using an FDM 3D printer. The printed structure after the compression test is shown in Figure 3.

Statistical tests were conducted to assess the significance of each model, individual model terms, and lack-of-fit in order to evaluate the generated model. The significance level was established at 0.05 for a factor to be deemed statistically significant. The analysis of variance (ANOVA) test results for compressive strength are presented in Table 3, providing detailed information. The analysis revealed a p-value of < 0.0001 for the model, indicating its statistical significance and desirability [22]. The primary factors that had a significant impact were the thickness of the layers (*A*), the rate at which the material flowed (*B*), and the density at which the material was filled (*C*). However, the pattern in which the material was filled (*D*) did not have a significant influence.

Table 2: Complete design layout of 4 factors 2-level factorial design and the responses obtained from the 3D printing process

Std. run no.	Run	Input factors				Responses	
		A- Layer thickness (mm)	*B*- Flow rate (%)	*C*- Filling density (%)	*D*- Filling pattern	Compressive strength (MPa)	Young's modulus (MPa)
1	7	1	25	1	5	0.748	15.546
2	10	5	25	1	5	0.522	13.988
3	16	1	35	1	5	0.631	14.765
4	1	5	35	1	5	0.412	13.166
5	11	1	25	2	5	0.783	16.221
6	2	5	25	2	5	0.681	14.336
7	19	1	35	2	5	0.775	16.021
8	15	5	35	2	5	0.564	13.773
9	13	1	25	1	11	0.684	15.662
10	4	5	25	1	11	0.544	13.881
11	8	1	35	1	11	0.62	14.403
12	17	5	35	1	11	0.433	13.248
13	20	1	25	2	11	0.787	16.558
14	3	5	25	2	11	0.733	14.533
15	6	1	35	2	11	0.747	16.113
16	18	5	35	2	11	0.584	13.809
17	14	3	30	1.5	8	0.589	14.753
18	9	3	30	1.5	8	0.537	14.531
19	5	3	30	1.5	8	0.544	14.788
20	12	3	30	1.5	8	0.577	14.992

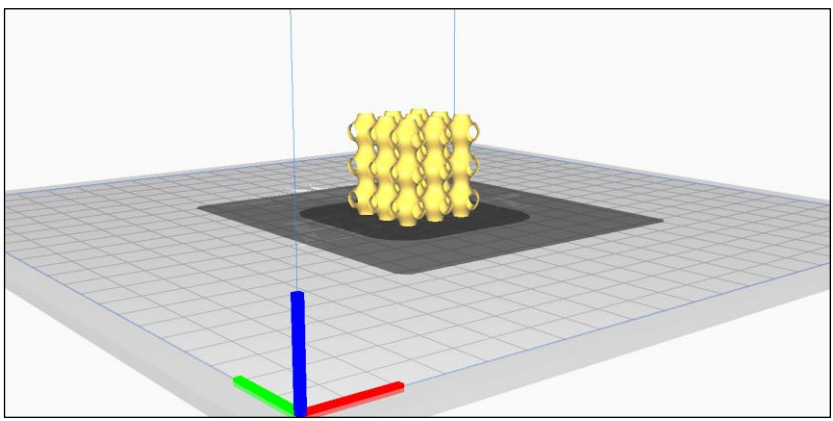

Figure 2: 3D scaffold structure in cura software for slicing and generating the G-Code

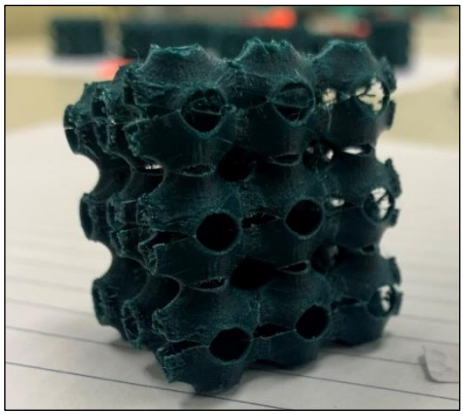

Figure 3: 3D printed TPMS scaffold after compression test

The p-value for lack-of-fit revealed that it was not statistically significant, and the model's adequacy in accounting for noise was 52.59%. The Model F-value of 62.30 indicated that the model is statistically significant. The model terms *A*, *B*, and *C* were deemed significant in this case.

Table 3: ANOVA results for compressive strength (MPa)

Source	**Sum of Squares**	**Degree of freedom**	**Mean Square**	**F value**	**p-value**	
Model	0.21	3	0.069	62.30	< 0.0001	significant
A-Layer thickness	0.11	1	0.11	95.11	< 0.0001	
B- Flow rate (%)	0.032	1	0.032	28.76	< 0.0001	
C-Filling density (%)	0.070	1	0.070	63.04	< 0.0001	
Curvature	0.020	1	0.020	17.81	0.0007	significant
Residual	0.017	15	1.114×10^{-3}			
Lack of fit	0.015	13	1.146×10^{-3}	1.26	0.5259	not significant
Pure Error	1.812×10^{-3}	2	9.062×10^{-4}			
Std. Dev.	0.033	R^2	0.9257			
Mean	0.62	Adj. R^2	0.9108			
C.V.	5.34	Pred R^2	0.8786			
PRESS	0.030	Adeq. Precision	23.055			

The obtained R^2 value was 0.9257, which indicates a high level of correlation and is considered good. The value indicated that the model accounted for approximately 92.57% of the variability in the answer. The forecasted R^2 value of 0.8786 was reasonably consistent with the neighbouring R^2 value of 0.9108. The signal-to-noise ratio is determined by the level of precision. A ratio over 4 is preferable. A signal with a ratio of 23.055 is considered sufficient. This paradigm is applicable for navigating the design space.

Equations (1) and (2) represented the ultimate empirical model for compressive strength, generated by the Design Expert software following the optimization process. These equations account for both coded and real components.

$$Compressive\ Strength = +0.64 - 0.081 * A - 0.045 * B + 0.066 * C \quad (1)$$

where *A* is the layer thickness, *B* is the flow rate, and *C* is the filling density.

$$Compressive\ Strength = +0.85904 - 0.46500 * Layer\ Thickness - 4.47500x10^{-3} * Flow\ rate + 2.20833x10^{-3} * Filling\ Density \quad (2)$$

Figure 4 depicts the normal probability plot of residuals, revealing that the residuals align in a linear pattern. This indicates that the errors follow a normal distribution, which is favorable for conducting parametric statistical tests and calculating confidence intervals.

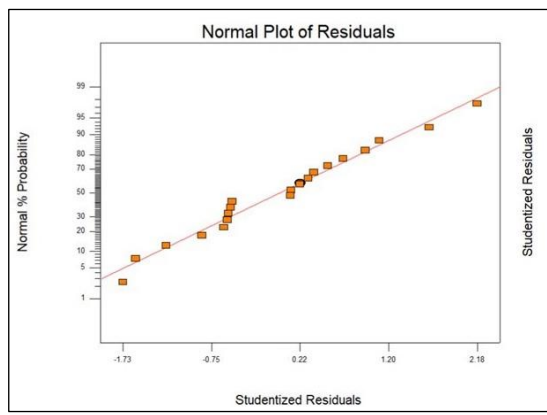

Figure 4: Adequacy checks for compressive strength in normal probability plot

Figure 5 shows the plot of residuals against anticipated values. The data exhibited no discernible structure and was distributed randomly. The graphic

indicated that the model's predictions exhibit no consistent errors across the whole range of predictions, which is advantageous for the model's application in forecasting the compressive strength of bone tissue engineering scaffolds. Based on the analysis of these two plots, it can be inferred that the estimated model was satisfactory and there is no evidence of a violation of the assumption of constant variance.

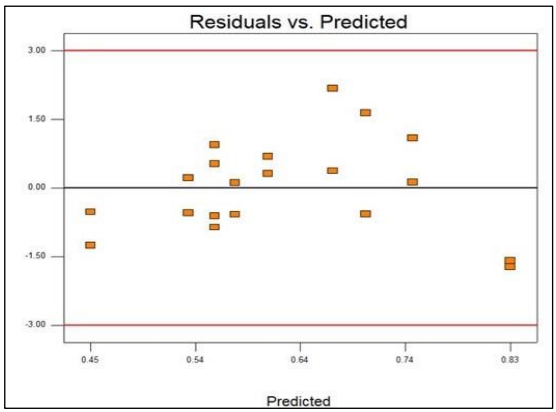

Figure 5: Adequacy checks for compressive strength in residual versus predicted values

Figure 6 illustrates the 3D surface plot for the significant factors. However, it can be seen that the optimal value of compressive strength exceeds the existing range of experiments. These results indicated that the compressive strength of bone scaffolds made using FDM 3D printing technology is influenced by crucial aspects such as layer thickness, flow rate, and filling density.

From Figures 7(a) to 7(c), the plots indicated that reducing the thickness of the layer could potentially enhance the robustness of the scaffolds. However, this adjustment must be carefully balanced with the flow rate, since it also has an impact on the strength of the scaffolds. Furthermore, an increased filling density consistently improves the compressive strength, which is vital for maintaining the structural integrity of bone scaffolds. The results obtained from these plots can provide valuable guidance for fine-tuning the FDM 3D printing parameters in order to maximize the compressive strength of bone scaffolds, hence ensuring their compliance with the necessary criteria for clinical application. The data emphasizes the need to carefully choose these characteristics to create a scaffold that has the required level of porosity and strength, which is necessary for effectively supporting bone regeneration.

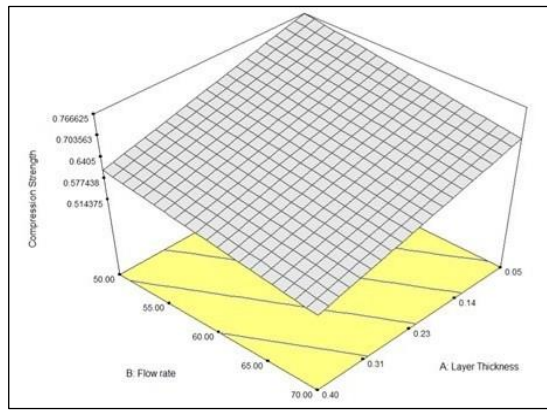

Figure 6: 3D Surface plot for compressive strength

Table 4 presents the specific information on the ANOVA test outcomes for Young's modulus. The analysis revealed a p-value of less than 0.0001, indicating a significant model. The primary factors that had a significant impact were the thickness of the layers (*A*), the rate at which the material flowed (*B*), and the density at which the material was filled (*C*). However, the pattern in which the material was filled (*D*) did not have a significant influence. The lack-of-fit P-value suggested that it was not statistically significant, and the model's adequacy in accounting for noise was 57.47%. The model F-value of 103.17 indicates that the model is statistically significant. In this instance, model terms *A*, *B*, and *C* held considerable significance.

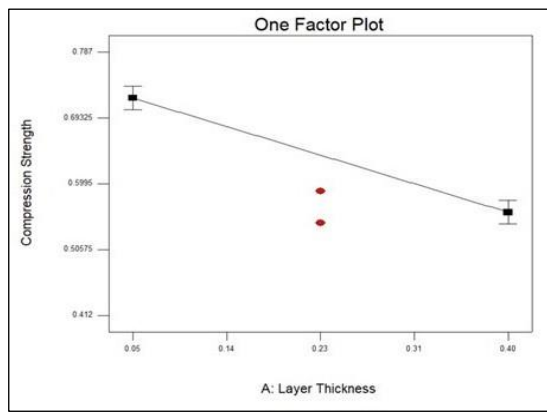

(a)

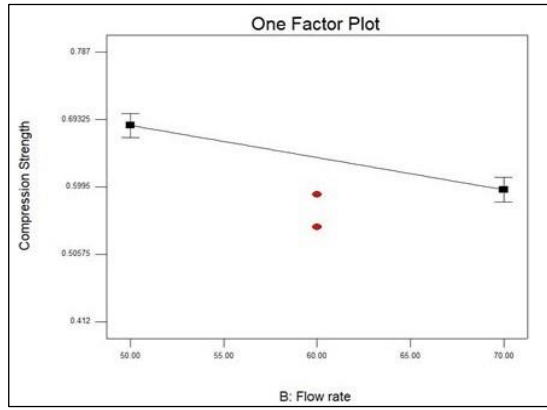

(b)

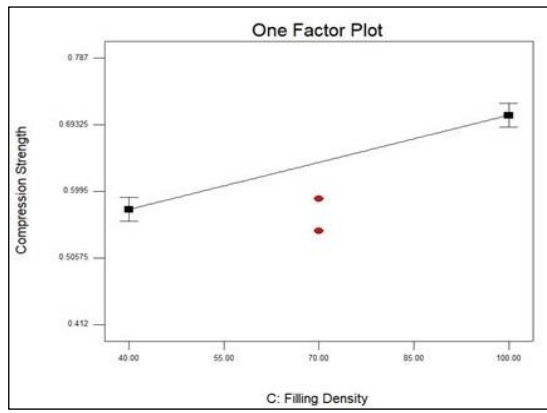

(c)

Figure 7. One factor plot for (a) layer thickness, (b) flow rate, and (c) filling density

The obtained R^2 value was 0.9538, indicating a high degree of correlation and desirability. The value indicated that the model accounted for approximately 95.38% of the variability in the answer. The projected R^2 value of 0.9178 was reasonably close to the nearby R^2 value of 0.9445. The signal-to-noise ratio is determined by the level of precision. A ratio over 4 is preferable. A signal with a ratio of 27.75 is considered sufficient. This paradigm is applicable for navigating the design space.

Table 4: ANOVA results for Young's modulus (MPa)

Source	Sum of squares	Degree of freedom	Mean square	F value	p-value	
Model	17.89	3	5.96	103.17	< 0.0001	significant
A-Layer thickness (mm)	13.24	1	13.24	229.05	< 0.0001	
B- Flow rate (%)	1.84	1	1.84	31.84	< 0.0001	
C-Filling density (%)	2.81	1	2.81	48.61	< 0.0001	
Curvature	6.786×10^{-4}	1	6.786×10^{-4}	0.012	0.9152	
Residual	0.87	15	0.058			
Lack of fit	0.76	13	0.058	1.09	0.5747	not significant
Pure error	0.11	2	0.053			
Std. Dev.	0.240431	R^2	0.953775			
Mean	14.75435	Adj. R^2	0.94453			
C.V.	1.629558	Pred. R^2	0.917825			
PRESS	1.541518	Adeq. precision	27.74916			

Equations (3) and (4) represent the ultimate empirical model for Young's modulus, generated by the Design Expert software following the optimization process. These equations incorporate both coded and real components.

$$Young's\ modulus = +14.75 - 0.91 * A - 0.34 * B + 0.42 * C \quad (3)$$

where *A* is the layer thickness, *B* is the flow rate and *C* is the filling density.

$$Young's\ modulus = +16.97835 - 5.19821 * Layer\ Thickness - 0.033919 * Flow\ rate + 0.013969 * Filling\ Density \quad (4)$$

Figure 8 represents a normal probability plot of residuals that exhibited linear alignment, showing their conformity to a normal distribution. This linear design is advantageous for conducting parametric statistical studies and for determining confidence intervals with enhanced precision.

Figure 9 illustrates a scatter plot depicting the residuals plotted against the expected values. The residuals exhibited a random distribution without any noticeable systematic structure. The presence of randomness in the scatter plot indicates that the predictive model is consistently accurate in making predictions across its whole range, without any noticeable consistent errors.

This is a valuable characteristic for its use in estimating the Young's Modulus of scaffolds for bone tissue engineering. The evaluation of these plots as a whole confirms that the predictive model is strong, and there are no evident breaches of the homoscedasticity assumption.

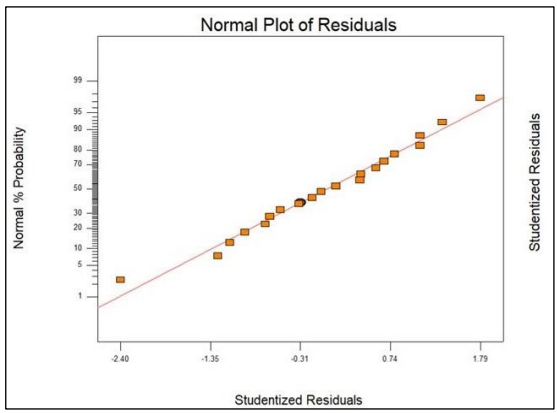

Figure 8. Adequacy checks for Young's modulus in a normal probability plot

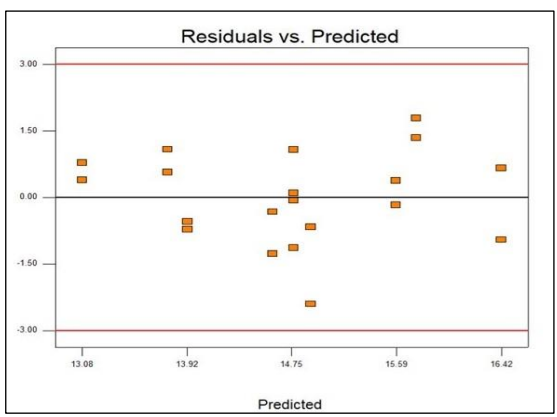

Figure 9. Adequacy checks for Young's modulus in residuals versus predicted values

Figure 10 depicts the 3D surface plot for the significant factors for Young's modulus. Young's modulus is a critical mechanical property that measures the stiffness of a solid material, indicating its ability to resist deformation under stress.

Figures 11(a) to 11(c) represent the plots for a single factor examining the influence of various manufacturing parameters on Young's modulus of bone scaffolds produced through 3D printing. The results depicted in this figure are vital for the optimization of 3D-printed bone scaffolds.

Both the response surface and one-factor plots indicated that the layer thickness and flow rate are important elements that must be precisely regulated in order to attain the desired mechanical properties, particularly the stiffness as measured by Young's modulus. The augmentation in layer thickness appeared to have an adverse impact on rigidity, potentially jeopardizing the structural soundness of the scaffold. On the other hand, increasing the filling density has a positive effect on Young's modulus, resulting in a stiffer scaffold that closely resembles the mechanical properties of genuine bone.

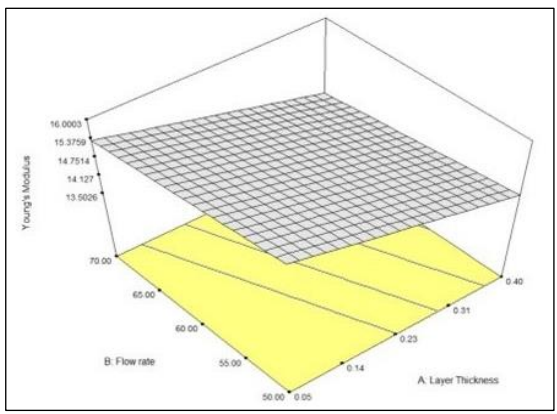

Figure 10: 3D surface plot for Young's modulus

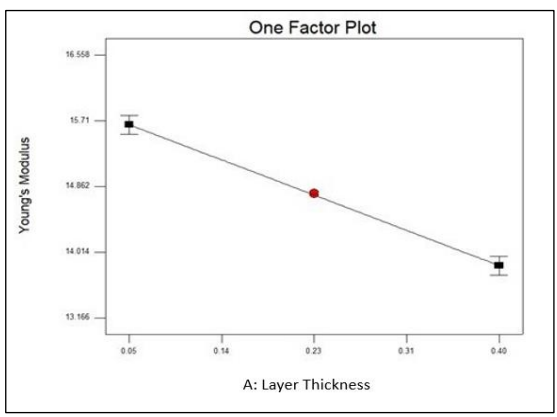

(a)

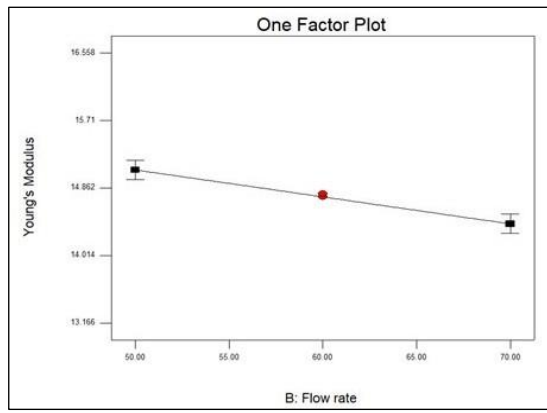

(b)

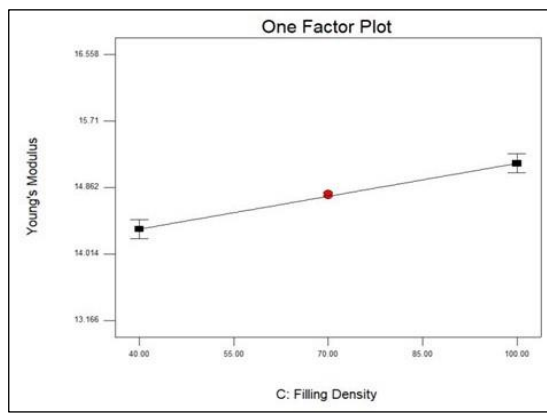

(c)

Figure 11: One-factor plot of (a) layer thickness (b) flow rate, and (c) filling density

These findings can be used to adjust the 3D printing parameters in actual applications to optimize the mechanical properties of bone scaffolds. Optimizing the layer thickness, flow velocity, and filling density can lead to scaffolds that are both structurally robust and favorable for cell attachment and proliferation, which is essential for successful bone tissue engineering [9], [18], [20].

Confirmation run

Six confirmation runs were conducted to validate the accuracy of the estimated model. The test circumstances for the first three confirmation runs were selected from the previously completed parameter settings, while the following three confirmation runs were chosen from unexplored conditions within the researched range.

The parameter values used in the experiments are presented in Table 5, which served as the basis for the results shown in Table 6. These parameter settings were employed to determine the compressive strength and Young's modulus values displayed in Table 6.

The experimental values for compressive strength and Young's modulus were predicted, accompanied by a 95% prediction interval. These predicted values and their respective intervals were derived from the developed models. A comparison between the predicted and experimental values was conducted, and the percentage error was calculated. The results are tabulated in Table 6. The percentage error for Young's modulus, comparing the actual values with the predicted ones, remained below 10%, which is within an acceptable range [23].

Table 5: Confirmation experiments parameter setting

No.	Layer thickness (mm)	Flow rate (%)	Filling density (%)	Filling pattern
1	0.05	50.00	100.00	Line
2	0.05	50.00	100.00	Rectangular
3	0.24	70.00	100.00	Line
4	0.24	70.00	100.00	Rectangular
5	0.05	50.00	40.00	Line
6	0.05	50.00	40.00	Rectangular

Table 6: Results of the Confirmation experiments compressive strength (MPa) and Young’s modulus (MPa) by using the parameter setting

No.	Compressive strength (MPa)			Young’s modulus (MPa)		
	Actual	Predicted	Error (%)	Actual	Predicted	Error (%)
1	0.857	0.832874	2.815	16.553	16.4194	0.80
2	0.826	0.832807	0.824	16.214	16.4189	1.263
3	0.677	0.654078	3.385	14.866	14.7427	0.829
4	0.684	0.653922	4.397	14.38	14.741	2.510
5	0.698	0.700375	0.340	15.611	15.5812	0.191
6	0.71	0.700472	1.341	16.705	15.5819	6.723

Discussion

The optimization of FDM 3D printing parameters is crucial for producing high-quality Triply Periodic Minimal Surfaces (TPMS) structures, which have been used increasingly in bone tissue engineering scaffolds due to their superior porosity and mechanical strength [5]. These structures are in high demand for bone tissue engineering scaffolds because of their exceptional porosity and mechanical strength. The results of the study indicated that the thickness of the layers, the rate at which the material flows, and the density at which the scaffold was filled are important elements that affect the mechanical characteristics of the printed scaffolds. Specifically, these factors substantially impact the compressive strength and Young's modulus of the scaffolds.

A 0.05 mm layer thickness in FDM 3D printing greatly improved the compressive strength and Young's modulus of bone scaffolds, especially those with TPMS architectures [6]. The enhancement can be ascribed to multiple interconnected elements intrinsic to the 3D printing procedure.

By reducing the layer thickness, it resulted in a more polished surface at the microscopic level. The smoothness is crucial because it minimizes the amount of tiny abnormalities on the surface of the scaffold that could potentially concentrate tension. Stress concentrators are specific locations inside a material where stress can gather, resulting in material collapse under loads that are lower than anticipated [11]. By reducing these possible vulnerabilities, the scaffold can endure higher stresses, hence improving its compressive strength.

The presence of finer layers results in a higher quantity of interlayer interfaces, which, when properly bonded, yield a more compact and uniform structure. The enhanced cohesion between layers guarantees a more uniform distribution of loads throughout the structure [21]. The even distribution of stress in this context adds to the overall structural integrity and improves Young's modulus, which indicates the material's ability to resist deformation when subjected to stress.

Enhanced regulation of layer thickness enables more accurate reproduction of the complex geometries found in TPMS structures, renowned for their optimal combination of strength and porosity. Precise duplication of these geometries guarantees the mechanical soundness of the scaffold's design, maximizing its ability to offer structural support [5], [24].

Using a layer thickness of 0.05 mm in 3D printing bone scaffolds enhances mechanical performance by enhancing surface quality, facilitating stronger bonding between layers, and preserving the integrity of intricate scaffold shapes [12]. These factors are crucial for creating dependable and efficient bone tissue engineering scaffolds.

Optimizing the flow rate at 50% during FDM 3D printing is crucial for attaining superior compressive strength and Young's modulus in bone

scaffolds, especially when compared to a flow rate of 100%. The controlled rate of flow is noteworthy for various reasons.

A flow rate of 50% allows for accurate regulation of the quantity of material being extruded, which is particularly crucial for preserving the accuracy of TPMS geometries. A precise material deposition is necessary for these structures in order to maintain their detailed patterns, which are essential for both mechanical stability and biological activity [25]. When the printer operates at a higher flow rate, such as 100%, there is a risk of excessive material extrusion. This can result in over-extrusion, causing the material to ooze, merge, or warp. As a consequence, the precision of the scaffold may be compromised, and the porous channels that are crucial for cell migration and nutrient diffusion may become obstructed.

Additionally, a decrease in flow rate leads to the formation of thinner material strands, which might undergo faster cooling and solidification. The rapid solidification promotes the formation of more robust connections between consecutive layers of the scaffold due to less thermal distortion. The robust bonding between layers plays a crucial role in determining the compressive strength of the scaffold, as it minimizes the occurrence of tiny gaps that may cause structural breakdown when subjected to a load [11].

Conversely, a flow rate of 100% may result in the deposition of an excessive amount of material that does not adhere well, leading to the formation of empty spaces and irregularities within the structure, thus compromising its mechanical integrity. The surplus material can also heighten the probability of flaws, such as unintentional porosity, which can undermine the compressive strength and rigidity of the scaffold.

Hence, a flow rate of 50% achieves a delicate equilibrium by supplying sufficient material to maintain the scaffold's structural integrity while preserving the intended porosity and intricate TPMS architecture. As a result, this results in the best mechanical characteristics, including increased ability to withstand compression and higher Young's modulus. These features are essential for the effective performance of scaffolds used in bone tissue engineering [26].

The observation that a filling density of 100% results in the maximum compressive strength and Young's modulus in bone scaffolds is based on the fundamental concepts of materials science and mechanical engineering. Filling density in 3D printing denotes the proportion of the print's internal volume occupied by material rather than empty or permeable. When the scaffold is filled at 100% density, it becomes entirely solid, with material occupying all available space within the specified print boundaries.

The complete filling of the scaffold with material greatly improves its ability to resist deformation when subjected to compressive stresses, resulting in a high compressive strength. The lack of empty spaces or openings inside the structure ensures that the applied load is evenly distributed over the whole volume of the scaffold. Every component of the material helps to support the

weight, resulting in a more robust structure as a whole [5]. Furthermore, the uninterrupted material phase guarantees the absence of vulnerable areas or stress concentrators that may trigger material breakdown, thereby enhancing the scaffold's capacity to endure mechanical loads.

A 100% filling density results in a homogenous and continuous material structure, as measured by Young's modulus, which quantifies a material's stiffness and its ability to deform elastically under applied stress. The homogeneity of the scaffold restricts the extent of elastic deformation it experiences when exposed to stress. The material exhibits a higher level of rigidity because of the absence of any porous regions that can absorb the energy from the applied force through deformation [27]. Consequently, the scaffold demonstrates an elevated Young's modulus, signifying increased stiffness and rigidity. These traits are especially sought after in bone scaffolds aiming to replicate the mechanical properties of real bone.

Nevertheless, this enhancement in mechanical characteristics entails considering the scaffold's biological functionality. Although a strong framework enhances the ability to withstand compression and rigidity, it can hinder the scaffold's biological performance. Porosity is an essential determinant in tissue engineering since it facilitates the movement of cells, diffusion of nutrients, and development of blood vessels inside the scaffold [16]. A scaffold that is filled with material does not have any porosity channels, which may restrict its ability to promote tissue growth and integration effectively [28]-[29]. Hence, although a greater filling density is advantageous in mechanics, it is crucial to strike a harmonious equilibrium between mechanical robustness and biological efficacy when designing bone tissue engineering scaffolds.

From this study, the filling patterns, including linear and rectangular, revealed no substantial disparity in their influence on the mechanical properties of the scaffold. These findings indicated that both filling schemes, when used within the limitations of the TPMS geometry, can effectively preserve the scaffold's structural integrity [30]-[31]. The lack of significant differences between linear and rectangular filling patterns in their impact on the mechanical properties of TPMS-based bone scaffolds may be attributed to various interconnected factors. Regarding stress distribution, both designs are expected to offer a similar framework enabling equitable stress allocation. Uniformity is crucial for scaffolds that need to withstand mechanical loads identical to those encountered by actual bone tissue. For infill efficiency, the internal space of the scaffold is filled by either design, if optimized, may lead to a comparable material density [20]. As a result, this results in similar mechanical properties independent of the selected pattern.

In addition, the intrinsic geometry of the TPMS structure itself has a significant influence, which may overshadow the effect of the infill pattern[9]. The TPMS design is principally accountable for the scaffold's mechanical and biological characteristics. If the selected infill pattern does not disrupt the

TPMS geometry, it is improbable that it will substantially impact these characteristics. Finally, ensuring material continuity is essential to prevent points of failure and uphold the mechanical integrity of the scaffold. Both linear and rectangular designs are very likely to guarantee sufficient material continuity, which is a crucial aspect of the scaffold's structural robustness [32]. Therefore, although the selection of the infill pattern may not significantly impact the mechanical properties of the scaffold, it is still a factor to be weighed against other considerations such as production efficiency and the intended purpose of the scaffold.

Conclusion

The mechanical properties of scaffolds for bone tissue engineering have been significantly improved by optimizing Fused Deposition Modeling (FDM) 3D printing settings, specifically a layer thickness of 0.05 mm, a flow rate of 50%, and a filling density of 100%. This has resulted in a compressive strength of 0.8329 MPa and Young's modulus of 16.42 MPa. These improvements are crucial for Triply Periodic Minimal Surface (TPMS) structures, as they necessitate precise manufacturing techniques to preserve their intricate geometry and structural integrity when subjected to physiological pressures. The confirmation tests have demonstrated an error margin that is less than 10%, indicating the great reliability and consistency of the scaffold quality. Although there have been advancements in mechanical strength, the increased filling density may negatively impact the porosity, which is crucial for cell development and tissue integration. This work highlights the notable progress in 3D printing and emphasizes the importance of achieving a delicate balance between mechanical strength and biological functionality in scaffold design for effective developments in bone tissue synthesis.

Contributions of Authors

The authors confirm the equal contribution in each part of this work. All authors reviewed and approved the final version of this work.

Funding

This research was funded by Ministry of Higher Education Malaysia under Fundamental Research Grant Scheme (FRGS) (FRGS/1/2024/TK10/UTM/02/8) (R.J130000.7824.5F739) and Universiti

Teknologi Malaysia (UTM) under the scheme UTMShine (Q.J130000.2451.09G94).

Conflict of Interests

All authors declare that they have no conflicts of interest.

Acknowledgment

The authors would like to acknowledge the financial support from the Ministry of Higher Education Malaysia and Universiti Teknologi Malaysia for the funding under UTMShine (Q.J130000.2451.09G94).

References

[1] A. Gregor, E. Filova, M. Novak, J. Kronek, H. Chlup, M. Buzgo, V. Lukasova, M. Bartos, A. Necas, and J. Hosek, "Designing of PLA scaffolds for bone tissue replacement fabricated by ordinary commercial 3D printer," *Journal of Biological Engineering*, vol. 11, no. 1, pp. 1–21, 2017.

[2] E. Davoodi, H. Montazerian, A. Khademhosseini, and E. Toyserkani, "Sacrificial 3D printing of shrinkable silicone elastomers for enhanced feature resolution in flexible tissue scaffolds", *Acta Biomaterialia*, vol. 117, pp. 261–272, 2020.

[3] A. Ghilan, A. P. Chiriac, L. E. Nita, A. G. Rusu, I. Neamtu, and V. M. Chiriac, "Trends in 3D printing processes for biomedical field: opportunities and challenges," *Journal of Polymers and the Environment*, vol. 28, pp. 1345–1367, 2020.

[4] Q. Yan, H. Dong, J. Su, J. Han, B. Song, Q. Wei, and Y. Shi "A review of 3D printing technology for medical applications", *Engineering*, vol. 4, no. 5, pp. 729–742, 2018.

[5] Z. Li, Z. Chen, X. Chen, and R. Zhao, "Design and evaluation of TPMS-inspired 3D-printed scaffolds for bone tissue engineering: Enabling tailored mechanical and mass transport properties", *Composite Structure*, vol. 327, pp. 1-14, 2024.

[6] W. Guo, Y. Yang, C. Liu, W. Bu, F. Guo, J. Li, E. Wang, Z. Peng, H. Mai, H. You, and Y. Long, "3D printed TPMS structural PLA/GO scaffold: Process parameter optimization, porous structure, mechanical and biological properties," *Journal of the Mechanical Behavior of Biomedical Materials*, vol. 142, pp. 1-13, 2023.

[7] A. Dey and N. Yodo, "A systematic survey of FDM process parameter optimization and their influence on part characteristics," *Journal of Manufacturing and Materials Processing*, vol. 3, no. 3, pp. 1-30, 2019.

[8] A. Nurulhuda, I. Sudin, and N. H. A. Ngadiman, "Fabrication a novel 3D tissue engineering scaffold of Poly (ethylene glycol) diacrylate filled with Aramid Nanofibers via Digital Light Processing (DLP) technique," *Journal of Mechanical Engineering*, vol. 9, pp. 1–12, 2020.

[9] M. Alizadeh-Osgouei, Y. Li, A. Vahid, A. Ataee, and C. Wen, "High strength porous PLA gyroid scaffolds manufactured via fused deposition modeling for tissue-engineering applications", *Smart Materials in Medicine*, vol. 2, pp. 15–25, 2021.

[10] D. A. De Aquino, I. Maskery, G. A. Longhitano, A. L. Jardini, and E. G. Del Conte, "Investigation of load direction on the compressive strength of additively manufactured triply periodic minimal surface scaffolds," *The International Journal of Advanced Manufacturing Technology*, vol. 109, pp. 771–779, 2020.

[11] U. Cevik and M. Kam, "A review study on mechanical properties of obtained products by FDM method and metal/polymer composite filament production," *Journal of Nanomaterials*, vol. 2020, pp. 1–9, 2020.

[12] V. E. Kuznetsov, A. N. Solonin, O. D. Urzhumtsev, R. Schilling, and A. G. Tavitov, "Strength of PLA components fabricated with fused deposition technology using a desktop 3D printer as a function of geometrical parameters of the process," *Polymers*, vol. 10, no. 3, pp. 1-9, 2018.

[13] L. Germain, C. A. Fuentes, A. W. van Vuure, A. des Rieux, and C. Dupont-Gillain, "3D-printed biodegradable gyroid scaffolds for tissue engineering applications," *Materials & Design*, vol. 151, pp. 113–122, 2018.

[14] N. H. A. Ngadiman, N. Mohd Yusof, A. Idris, and D. Kurniawan, "Mechanical properties and biocompatibility of co-axially electrospun polyvinyl alcohol/maghemite", *Proceedings of the Institution of Mechanical Engineers, Part H: Journal of Engineering in Medicine*, vol. 230, no. 8, pp. 739–749, 2016.

[15] N. H. A. Ngadiman, N. Mohd Yusof, A. Idris, D. Kurniawan, and E. Fallahiarezoudar, "Fabricating high mechanical strength γ-Fe 2 O 3 nanoparticles filled poly(vinyl alcohol) nanofiber using electrospinning process potentially for tissue engineering scaffold," *Journal of Bioactive and Compatible Polymers*, vol. 32, no. 4, pp. 411–428, 2017. doi: 10.1177/0883911516681328

[16] N. H. A. Ngadiman, N. M. Yusof, A. Idris, E. Misran, and D. Kurniawan, "Development of highly porous biodegradable γ-Fe2O3/polyvinyl alcohol nanofiber mats using electrospinning process for biomedical

application", *Materials Science and Engineering: C*, vol. 70, pp. 520–534, 2017.

[17] G. Adikari Appuhamillage, "New 3D Printable Polymeric Materials for Fused Filament Fabrication (FFF)," PhD Thesis, Chemistry, The University of Texas at Dallas, 2018.

[18] B. Shaqour, M. Abuabiah, S. A. Fattah, A. Juaidi, R. Abdallah, W. M. Abuzaina, M. Alqarout, B. Verleije, and P. Cos, "Gaining a better understanding of the extrusion process in fused filament fabrication 3D printing: a review," *The International Journal of Advanced Manufacturing Technology*, vol. 114, pp. 1279–1291, 2021.

[19] S. Eftekhari, I. El Sawi, Z. S. Bagheri, G. Turcotte, and H. Bougherara, "Fabrication and characterization of novel biomimetic PLLA/cellulose/hydroxyapatite nanocomposite for bone repair applications", *Materials Science and Engineering: C*, vol. 39, pp. 120–125, 2014.

[20] W. Wang, P. Liu, B. Zhang, X. Gui, X. Pei, P. Song, X. Yu, Z. Zhang, and C. Zhou, "Fused Deposition Modeling Printed PLA/Nano β-TCP Composite Bone Tissue Engineering Scaffolds for Promoting Osteogenic Induction Function," *International Journal of Nanomedicine*, vol. 18, pp. 5815–5830, 2023.

[21] N. M. Raffic, K. G. Babu, S. Selvakumar, and S. Radhakrishnan, "Experimental Investigation on the Effect of Fused Deposition Modelling Parameters for HIPS Material by Experimental Design and MRO Techniques," in *IOP Conference Series: Materials Science and Engineering*, vol. 988, no. 1, pp. 1-20, 2020.

[22] N. H. A. Ngadiman, N. Mohd Yusof, A. Idris, D. Kurniawan, and E. Fallahiarezoudar, "Fabricating high mechanical strength γ-Fe2O3 nanoparticles filled poly (vinyl alcohol) nanofiber using electrospinning process potentially for tissue engineering scaffold," *Journal of Bioactive and Compatible Polymers*, vol. 32, no. 4, pp. 411–428, 2017.

[23] N. H. A. Ngadiman, R. Z. Abidin, N. I. S. Murizan, N. M. Yusof, A. Idris, and A. Z. A. Kadir, "Optimization of materials composition and uv-vis light wavelength towards curing time performance on development of tissue engineering scaffold", *Biointerface Research in Applied Chemistry*, vol. 11, pp. 8740–8750, 2020.

[24] A. P. G. Castro, T. Pires, J. E. Santos, B. P. Gouveia, and P. R. Fernandes, "Permeability versus design in TPMS scaffolds", *Materials*, vol. 12, no. 8, pp. 1-7, 2019.

[25] A. Nurulhuda, S. Izman, and N. H. A. Ngadiman, "Fabrication PEGDA/ANFs biomaterial as 3D tissue engineering scaffold by DLP 3D printing technology," *International Journal of Engineering and Advanced Technology*, vol. 8, pp. 751–758, 2019.

[26] S. Toosi, M. J. Javid-Naderi, A. Tamayol, M. H. Ebrahimzadeh, S. Yaghoubian, and S. A. Mousavi Shaegh, "Additively manufactured

porous scaffolds by design for treatment of bone defects", *Frontiers in Bioeng and Biotechnology*, vol. 11, pp. 1-17, 2024.

[27] Y. Jia, H. He, X. Peng, S. Meng, J. Chen, and Y. Geng, "Preparation of a new filament based on polyamide-6 for three-dimensional printing", *Polymer Engineering and Science*, vol. 57, no. 12, pp. 1322–1328, 2017.

[28] X.-Y. Yang, L.-H. Chen, Y. Li, J. C. Rooke, C. Sanchez, and B.-L. Su, "Hierarchically porous materials: synthesis strategies and structure design", *Chemical Society Reviews*, vol. 46, no. 2, pp. 481–558, 2017.

[29] Z. Zhang, H. Zhang, J. Zhang, S. Qin, and M. Duan, "Study on flow field characteristics of TPMS porous materials," *Journal of the Brazilian Society of Mechanical Sciences and Engineering*, vol. 45, no. 188, pp.188 , 2023.

[30] U. Simsek, A. Akbulut, C. E. Gayir, C. Basaran, and P. Sendur, "Modal characterization of additively manufactured TPMS structures: comparison between different modeling methods," *The International Journal of Advanced Manufacturing Technology*, vol. 115, pp. 657–674, 2021.

[31] N. Novak, O. A. -Ketan, L. K. -Opara, R. Rowshan, R. K. A. -Rub, M. Vesenjak, and Z. Ren, "Quasi-static and dynamic compressive behaviour of sheet TPMS cellular structures", *Composite Structures*, vol. 266, pp. 1-10, 2021.

[32] C. N. Kelly, A. T. Miller, S. J. Hollister, R. E. Guldberg, and K. Gall, "Design and structure--function characterization of 3D printed synthetic porous biomaterials for tissue engineering", *Advanced Healthcare Materials*, vol. 7, no. 7, pp. 1-16, 2018.